Restacked Perovskite Nanosheets and Their Pt-Loaded Materials as Photocatalysts

Yasuo Ebina,* Takayoshi Sasaki, Masaru Harada, and Mamoru Watanabe

Advanced Materials Laboratory, National Institute for Materials Science, 1-1 Namiki, Tsukuba, Ibaraki, 305-0044, Japan

Received May 28, 2002. Revised Manuscript Received July 29, 2002

Colloidal perovskite nanosheets of $[Ca_2Nb_3O_{10}]^-$ were reassembled by flocculation with aqueous solutions containing alkali metal ions. X-ray diffraction and chemical analysis data on the derived products indicated that a limited number of nanosheets were restacked in such a way as to restore a layered structure that accommodated alkali metal ions and water molecules between the nanosheets. This exfoliation/restacking process resulted in porous aggregates of fine crystallites with high specific surface areas compared to those of the original layered perovskite. The aggregates showed high photocatalytic activity for hydrogen gas generation from an aqueous methanol solution. A maximum evolution rate of 550 μmol h^{-1} was achieved at an optimum loading of Pt, which is higher than $KCa_2Nb_3O_{10}$ (63 μmol h^{-1}) and P-25 titanium oxide (390 μmol h^{-1}). Photoirradiation of a colloidal nanosheet suspension containing H_2PtCl_6 allowed direct deposition of Pt nanoparticles on the surfaces of single-layer nanosheets. Pt single crystals as small as 1 nm were loaded onto nanosheets when Pt loading was 0.1 wt %, while larger polycrystalline particles of up to 10 nm were deposited when Pt loading was 3 wt %. The Pt-loaded nanosheets were flocculated with alkali metal ions, and the resulting aggregates showed a maximum activity of 900 μmol h^{-1} for hydrogen generation when Pt loading was 0.1 wt %.

Introduction

Several classes of layered host materials are known to act as photocatalysts. A layered niobate of $K_4Nb_6O_{17}$ can efficiently split H_2O into H_2 and O_2 under band gap illumination.[1] It has also been reported that a series of layered titanates and layered perovskites (e.g., $Na_2Ti_3O_7$, $K_2Ti_4O_9$, $K_2La_2Ti_3O_{10}$, and $KCa_2Nb_3O_{10}$) exhibit photocatalytic activities.[2−5] These layered materials are comprised of semiconducting host layers and interlayer alkali cations. Charge separation takes place in the host layers upon ultraviolet irradiation. The generated electrons and holes show high reductive and oxidative reactivities, which is the origin of photocatalytic properties. The interlayer guests are ion-exchangeable with various foreign species.[6] Cationic species such as Ni^{2+} and $Pt(NH_3)_4^{2+}$ have been introduced into interlayer galleries as precursors of photocatalytically active sites.[7] Although ion-exchange reactions provide facile and powerful tools in chemical modification of photocatalysts, they continue to suffer from a limitation of cations for use. Some ions are difficult to incorporate into the hosts due to the chemical nature or steric hindrance of these ions.

The layered host materials mentioned above undergo exfoliation upon interacting with bulky guests, for example, quaternary ammonium ions.[8−12] The resulting unilamellar crystallites can be regarded as a new family of nanosized semiconductors. These so-called "nanosheet semiconductors" have a thickness of ≈1 nm that is comparable to the dimensions of molecules.[13] In con-

* To whom correspondence should be addressed. E-mail: ebina.yasuo@nims.go.jp. Fax: +81-298-54-9061.

(1) (a) Domen, K.; Kudo, A.; Shinozaki, A.; Tanaka, A.; Maruya, K.; Onishi, T. *Chem. Commun.* **1986**, 1706. (b) Kudo, A.; Sayama, K.; Tanaka, A.; Domen, K.; Maruya, K.; Onishi, T. *J. Catal.* **1990**, *124*, 541. (c) Sayama, K.; Arakawa, H.; Domen, K. *Catal. Today* **1996**, *28*, 175.

(2) Shibata, M.; Kudo, A.; Tanaka, A.; Domen, K.; Maruya, K.; Onishi, T. *Chem. Lett.* **1987**, 1017.

(3) (a) Takata, T.; Furumi, Y.; Shinohara, K.; Tanaka, A.; Hara, M.; Kondo, J. N.; Domen, K. *Chem. Mater.* **1997**, *9*, 1063. (b) Takata, T.; Shinohara, K.; Tanaka, A.; Hara, M.; Kondo, J. N.; Domen, K. *J. Photochem. Photobiol. A* **1997**, *106*, 45. (c) Ikeda, S.; Hara, M.; Kondo, J. N.; Domen, K. *Chem. Mater.* **1998**, *10*, 72. (d) Ikeda, S.; Hara, M.; Kondo, J. N.; K. Domen, Takahashi, H.; Okubo, T.; Kakihana, M. *J. Mater. Res.* **1998**, *13*, 852.

(4) (a) Domen, K.; Yoshimura, J.; Sekine, T.; Tanaka, A.; Onishi, T. *Catal. Lett.* **1990**, *4*, 339. (b) Domen, K.; Ebina, Y.; Sekine, T.; Tanaka, A.; Kondo, J.; Hirose, C. *Catal. Today* **1993**, *16*, 479. (c) Ebina, Y.; Tanaka, A.; Kondo, J. N.; Domen, K.; *Chem. Mater.* **1996**, *8*, 2534.

(5) (a) Kim, Y. I.; Salim, S.; Huq, M. J.; Mallouk, T. E. *J. Am. Chem. Soc.* **1991**, *113*, 9561. (b) Kim, Y. I.; Atherton, S. J.; Brigham, E. S.; Mallouk, T. E. *J. Phys. Chem.* **1993**, *97*, 11802.

(6) Clearfield, A. *Chem. Rev.* **1988**, *88*, 125.

(7) (a) Kudo, A.; Tanaka, A.; Domen, K.; Maruya, K.; Aika, K.; Onishi, T. *J. Catal.*, **1988**, *111*, 67. (b) Sayama, K.; Tanaka, A.; Domen, K.; Maruya, K.; Onishi, T. *J. Phys. Chem.* **1991**, *95*, 1345.

(8) Treacy, M. M.; Rice, S. B.; Jacobson, A. J.; Lewandowski, J. T. *Chem. Mater.* **1990**, *2*, 279.

(9) Keller, S. W.; Kim, H.-N.; Mallouk, T. E. *J. Am. Chem. Soc.* **1994**, *116*, 8817.

(10) Fang. M.; Kim, C. H.; Saupe, G. B.; Kim, H.-N.; Waraksa, C. C.; Miwa, T.; Fujishima, A.; Mallouk, T. E. *Chem. Mater.* **1999**, *11*, 1526.

(11) (a) Sasaki, T.; Watanabe, M.; Hashizume, H.; Yamada, H.; Nakazawa, H. *J. Am. Chem. Soc.* **1996**, *118*, 8329. (b) Sasaki, T.; Watanabe, M. *J. Am. Chem. Soc.* **1998**, *120*, 4682. (c) Sasaki, T. Novel Nanosheet Crystallites and Their Layer-by-Layer Assembly. In *Handbook of Polyelectrolytes and Their Applications*; Tripathy S., Kumar, J., Nalwa H. S., Eds.; American Scientific Publishers: Stevenson Ranch, 2002; Vol. 1, pp 241−263.

(12) Harada, M.; Sasaki, T.; Ebina, Y.; Watanabe, M. *J. Photochem. Photobiol., A* **2002**, *148*, 273.

(13) Sasaki, T.; Ebina, Y.; Kitami, Y.; Watanabe, M.; Oikawa, T. *J. Phys. Chem. B* **2001**, *105*, 6116.

10.1021/cm020622e CCC: $22.00
Published on Web 09/07/2002

trast, the lateral size of these semiconductors is much larger, typically ≈1 μm, basically depending on the dimensions of the starting layered crystals.[13] This structural aspect is expected to lead to novel or enhanced physical properties. For example, nanosheets of titanium oxide exhibit a sharp and intense optical absorption at 265 nm, which is distinctly different from bulk titanium dioxide such as anatase and rutile.[14]

These nanosheet crystallites are very interesting from the viewpoint of material synthesis because they can be used as building blocks to construct a variety of nanostructured systems. Multilayer ultrathin films of various composition and architecture have been fabricated via electrostatic self-assembly using appropriate polyelectrolytes as counterions.[9,10,12,15,16] Formation of novel shapes such as thin flakes and hollow microspheres by using the nanosheets as building blocks has been achieved by applying freeze-drying or spray-drying processing.[17]

The colloidal nanosheets undergo flocculation to form a restacked product by changing the ionic strength or pH of the suspensions.[18] Using this simple procedure, it is possible to incorporate a range of guest species into the nanosheet gallery more easily than by ion-exchange reactions. A restacked product is characterized by its loose structure. The size of a crystallite is small, particularly along the stacking direction due to a limited number of restacked nanosheets. In addition, the stacking sequence is usually disordered. These structural features are expected to work favorably in designing high-performance catalysts. However, to the best of our knowledge, few studies have reported fabrication of photocatalysts via exfoliation and subsequent restacking despite the high catalytic activities reported for layered hosts. The present study was, therefore, undertaken to demonstrate the validity of this synthetic strategy. The typical layered perovskite of $KCa_2Nb_3O_{10}$ was exfoliated into nanosheets and then flocculated to produce restacked aggregates. Pt metal nanoparticles acting as active sites for photocatalytic activities were introduced directly onto the nanosheets themselves as well as onto the restacked aggregates. Decomposition of H_2O was examined using these materials as photocatalysts.

Experimental Section

Reagents and Materials. Reagents such as K_2CO_3, $CaCO_3$, and Nb_2O_5 were of 99.9% purity or higher (Rare Metallic Co.). All the other chemicals were of analytical grade. All water used in the experiments was purified to a resistivity of >17 MΩ cm by filtration through a Milli-Q reagent water system.

The starting material of $KCa_2Nb_3O_{10}$ was prepared according to the literature:[19] K_2CO_3, $CaCO_3$, and Nb_2O_5 were mixed at the ratio of 1.1:2:3 and calcined at 1473 K for 10 h. The obtained powder of $KCa_2Nb_3O_{10}$ (20 g) was treated with 500 cm^3 of HNO_3 aqueous solution (5 mol dm^{-3}) for 72 h. The product was recovered by filtration, washed with water, and air-dried. The resulting H^+-exchanged phase, $HCa_2Nb_3O_{10}\cdot 1.5H_2O$ (0.6 g), was shaken in an aqueous solution (150 cm^3) containing tetrabutylammonium hydroxide (TBAOH).[10,20,21] The concentration of the TBA solution was 7.3 mmol dm^{-3}, which is a favorable condition for promoting delamination of layered perovskite into colloidal single layers.

Pt Loading onto Nanosheets. The colloidal suspension of perovskite nanosheets (150 cm^3) was added into a solution of water (150 cm^3) and methanol (30 cm^3), into which 1.2−48 mg of H_2PtCl_6 had been dissolved. The dissolved amount corresponded to 0.1−3 wt % Pt with respect to $HCa_2Nb_3O_{10}\cdot 1.5H_2O$. The solution was stirred in a Pyrex reaction cell and irradiated during stirring with a 500 W Xe lamp for 30 min in an Ar atmosphere (about 13 kPa) for the photodeposition of Pt onto the nanosheets.

Flocculation of Nanosheets. Typically, 300 cm^3 of nanosheet colloidal suspension was added to 300 cm^3 of NaOH or KOH aqueous solution (2 mol dm^{-3}) at a drop rate of ≈1 cm^3 min^{-1}. The resulting precipitate was filtered, washed with water, and dried in air. The flocculated product is hereafter expressed as *ex*-$Ca_2Nb_3O_{10}/A^+$ where A = Na or K. Pt-loaded nanosheets were flocculated in the same way as nanosheets without Pt to obtain a reassembled aggregate.

Photocatalytic Reaction. Hydrogen generation from an aqueous methanol solution was performed as follows: An aggregate of reassembled nanosheets (0.1 g) was suspended in 300 cm^3 of an aqueous methanol solution (10 vol %) in an air-free closed gas circulation system with a reaction cell made of Pyrex glass (350 cm^3 capacity) that allows for outside irradiation. The system was photoirradiated with a 500 W Xe lamp under an Ar atmosphere (≈13 kPa). The evolved H_2 gas was determined by gas chromatography (MS-5A column, Ar carrier) through a gas sampler (7 cm^3) directly connected to the reaction system to avoid any contamination from the air.

Instrumentation. Transmission electron microscope (TEM) images at low magnification were obtained with a JEOL JEM-1010 operating at an accelerating voltage of 100 kV. High-resolution images and elemental analysis data by energy-dispersive X-ray analysis (EDX) were obtained by a JEOL JEM-3000F (accelerating voltage: 300 kV). Specimens were prepared by placing a drop of the diluted colloidal suspension onto a carbon-coated copper grid. After standing for 30 min, the suspension was removed. A Hitachi S-5000 scanning electron microscope was used for the morphological observation of the reassembled aggregates of nanosheets. The sample was deposited with Os to prevent charging.

The BET surface area was measured with a BELSORP 28SA. The sample was pretreated by evacuation at 473 K. Differential thermal analysis and thermogravimetry were carried out with a Rigaku TG8120 thermal analyzer at a heating rate of 10 K min^{-1} in air.

Chemical analysis was carried out by completely dissolving a weighed amount of sample in a mixed acid solution of concentrated H_2SO_4 and HF and subsequently determining K, Ca, and Nb by ICP-AES (Seiko 1700HVR). Powder X-ray diffraction (XRD) data were collected using a Rigaku Rint 2000S X-ray diffractometer with graphite monochromatized Cu Kα radiation (λ = 0.15405 nm).

Results and Discussion

Reassembling of Perovskite Nanosheets with Alkali Metal Ions. The colloidal nanosheet suspension

(14) Sasaki, T.; Watanabe, M. *J. Phys. Chem. B* **1997**, *101*, 10159.
(15) (a) Kaschak, D. M.; Johnson, S. A.; Hooks, D. E.; Kim, H.-N.; Ward, M. D.; Mallouk, T. E. *J. Am. Chem. Soc.* **1998**, *120*, 10887. (b) Kerimo, J.; Adams, D. M.; Barbara, P. F.; Kaschak, D. M.; Mallouk, T. E. *J. Phys. Chem. B* **1998**, *102*, 9451. (c) Kim. H.-N.; Keller, S. W.; Mallouk, T. E.; Schmitt, J.; Decher, G. *Chem. Mater.* **1997**, *9*, 1414.
(16) (a) Sasaki, T.; Ebina, Y.; Watanabe, M.; Decher, G. *Chem. Commun.* **2000**, 2163. (b) Sasaki, T.; Ebina, Y.; Tanaka, T.; Harada, M.; Watanabe, M.; Decher, G. *Chem. Mater.* **2001**, *12*, 4661. (c) Yamaki, T.; Asai, K. *Langmuir* **2001**, *17*, 2567.
(17) (a) Sasaki, T.; Nakano, S.; Yamauchi, S.; Watanabe, M. *Chem. Mater.* **1997**, *9*, 602. (b) Iida, M.; Sasaki, T.; Watanabe, M. *Chem. Mater.* **1998**, *10*, 3780.
(18) Jacobson, A. J. *Mater. Sci. Forum* **1994**, *152*, 1.
(19) (a) Dion, M.; Ganne, M.; Tournoux, M. *Mater. Res. Bull.* **1981**, *16*, 1429. (b) Jacobson, A. J.; Johnson, J. W.; Lewandowski, J. T. *Inorg. Chem.* **1985**, *24*, 3727.
(20) (a) Kaschak, D. M.; Lean, J. T.; Waraksa, C. C.; Saupe, G. B.; Usami. H.; Mallouk, T. E. *J. Am. Chem. Soc.* **1999**, *121*, 3435. (b) Schaak, R. E.; Mallouk, T. E. *Chem. Mater.* **2000**, *12*, 2513. (c) Schaak, R. E.; Mallouk, T. E. *Chem. Mater.* **2000**, *12*, 3427.
(21) Ebina, Y.; Sasaki, T.; Watanabe, M. *Solid State Ionics*, in press.

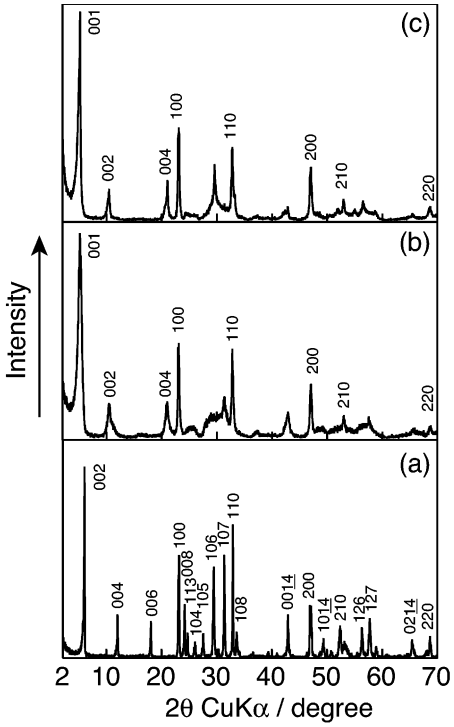

Figure 1. XRD patterns of the (a) starting material of $KCa_2Nb_3O_{10}$ and reassembled products obtained by flocculation with (b) K^+ and (c) Na^+.

Table 1. Elemental Analysis Results and BET Surface Areas of Aggregates and Starting Compound

	ratio of element			
	K or Na	Ca	Nb	BET surface area ($m^2\ g^{-1}$)
ex-$Ca_2Nb_3O_{10}/K^+$[a]	0.95	2.0	3.0	27
ex-$Ca_2Nb_3O_{10}/Na^+$	0.87	2.0	3.0	29
$KCa_2Nb_3O_{10}$	1.0	2.0	3.0	3

[a] K^+ in *ex*-$Ca_2Nb_3O_{10}/K^+$ means that the nanosheet was flocculated with K^+.

immediately underwent flocculation when added to an aqueous alkali hydroxide solution, yielding a precipitate at the bottom of the flask. Elemental analysis of the products (Table 1) revealed that the Ca/Nb ratio remained virtually unchanged while a slight reduction in alkali metal content was observed compared to the stoichiometric ratio of the precursor layered perovskite, that is, K/Ca/Nb = 1/2/3. The XRD patterns of the products were basically comprised of 00*l* basal series and *hk*0 reflections (see Figure 1). These diffraction features are attributed to the stacking of nanosheets and the two-dimensional atomic arrangement in the nanosheets, respectively. These structural and compositional data strongly suggest that the obtained precipitates were produced via restacking of the nanosheets. The basal spacing was ≈1.7 nm, which was about 0.2 nm larger than that of the starting compound of $KCa_2Nb_3O_{10}$. These results can be understood in terms of hydration. The sample was dehydrated by heating to 373 K, as indicated by the large weight loss accompanied by an endothermic peak. No noticeable thermal events were observed above 373 K. (Thermal analysis data is deposited as Supporting Information). The sample heated to 1273 K was composed mainly of $KCa_2Nb_3O_{10}$ with $Ca_2Nb_2O_7$ in a trace amount. The

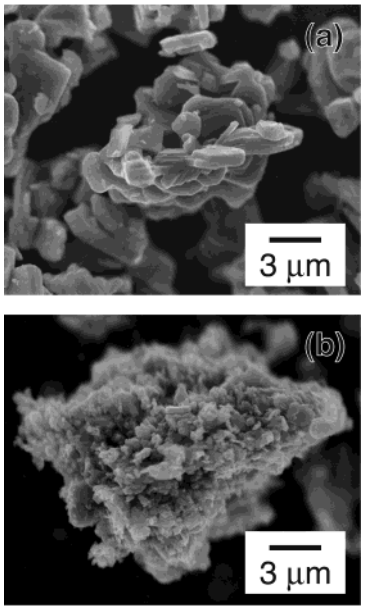

Figure 2. Scanning electron micrographs of (a) $KCa_2Nb_3O_{10}$ and (b) restacked aggregates, *ex*-$Ca_2Nb_3O_{10}/K^+$.

Table 2. Crystallite Size of Aggregates and Starting Compound

	coherent length (nm)	
	(001)	(100)
ex-$Ca_2Nb_3O_{10}/K^+$	7.2	29
ex-$Ca_2Nb_3O_{10}/Na^+$	13	31
$KCa_2Nb_3O_{10}$	>200	68

formation of $Ca_2Nb_2O_7$ is ascribed to the slight deficiency of alkali metal ions with respect to stoichiometry. The alkali deficiency may be compensated for by protons, most likely in the form of oxonium ions. The possibility of the presence of TBA ions can be ruled out since thermal analysis did not show an exothermic peak within the range of 573−673 K, where a peak would be expected to appear if an organic substance was included in the sample. The protons would be liberated as H_2O, removing oxygen atoms from the $Ca_2Nb_3O_{10}$ nanosheet and subsequently resulting in $Ca_2Nb_2O_7$.

The XRD data above evidently indicate that the exfoliation/restacking process introduces disorder into the structure as well as reduces the crystallite size. First, turbostratic stacking of perovskite nanosheets is suggested since only basal diffraction series of 00*l* and intra-nanosheet reflections of *hk*0 were observed. All general *hkl* lines were absent, indicating the loss of three-dimensional order. In addition, the line width (fwhm) of the basal reflections was much larger than that before exfoliation. The coherent lengths calculated on the basis of the Sherrer equation were found to be considerably smaller than those calculated for the starting material of $KCa_2Nb_3O_{10}$ (Table 2). Reduction of the crystallite size along the stacking direction was particularly significant. These dimensions correspond to stacks of four to eight nanosheets.

Figure 2 depicts the morphologies for the precursor compound (before delamination) and the flocculated product. The former are of platelike microcrystals submicrometer thick and several micrometers wide. In contrast, the latter is an agglomerate of very small particles. The drastic morphological change upon exfo-

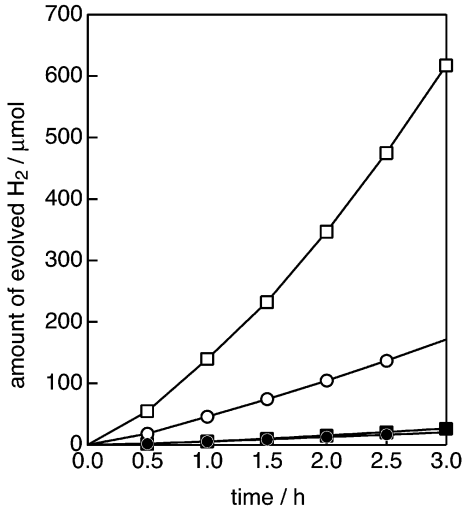

Figure 3. Hydrogen gas generation from aqueous methanol solutions: (■) restacked aggregates, *ex*-$Ca_2Nb_3O_{10}/K^+$; (□) *ex*-$Ca_2Nb_3O_{10}/K^+$ with Pt loading of 0.1 wt %; (●) starting compound of $KCa_2Nb_3O_{10}$; (○) $KCa_2Nb_3O_{10}$ with Pt loading of 0.1 wt %.

liation and reassembling enhances the BET surface area by ≈10 times (Table 1).

The observed weight loss upon heating corresponds to 6 mol of H_2O per $Ca_2Nb_3O_{10}$. As mentioned above, the interlayer distance increased by only 0.2 nm compared with the that of the anhydrous phase. From the viewpoint of crystal chemistry, this interlayer expansion cannot explain the accommodation of such a large amount of H_2O molecules in the nanosheet galleries. This implies that a majority of H_2O is adsorbed by possible pores in the aggregate. In fact, the dehydrated aggregate underwent quick rehydration upon contact with moist air, suggesting the presence of pores that adsorb H_2O molecules reversibly.

This synthetic route via exfoliation and subsequent restacking leads to a porous aggregate with a high specific surface area, which is remarkably different from the bulk material before delamination. The aggregate itself is composed of restacked nanosheets that accommodate alkali ions and water molecules between the layers.

Water Splitting with Restacked Aggregates under UV Irradiation. The high-surface-area layered perovskite associated with a stacking disorder and very small crystallite size is expected to result in the enhancement of the catalytic activity. Figure 3 shows the H_2 gas evolution rate when an aqueous methanol solution was photodecomposed in the presence of the aggregated sample as a photocatalyst. Without Pt loading, both the bulk starting compound $KCa_2Nb_3O_{10}$ and the restacked material *ex*-$Ca_2Nb_3O_{10}/K^+$ showed only modest H_2 generation of 7.7 and 11 μmol h^{-1}, respectively. When Pt was loaded (0.1 wt %) as active sites for H_2 generation, the photocatalytic activity for both materials showed great improvement. Figure 4 shows H_2 generation activity as a function of the amount of Pt loaded. It can clearly be seen that the restacked aggregates exhibit much higher photocatalytic activity than the bulk compound. The activity of the restacked aggregates was comparable to or even higher than that of TiO_2 (P-25, Japan Aerosil), which is well-known for its high photocatalytic activity. Another noteworthy point is that the optimum amount of Pt was different between the bulk compound and the restacked aggregate. The former, $KCa_2Nb_3O_{10}$, showed a maximum activity at 0.1 wt % of Pt loading while the restacked aggregates showed a maximum at 1 wt %. We attribute this difference in optimum Pt loading to a difference in the surface area. There might be an optimum ratio of Pt loading to surface area for these catalysts. Since the surface area of the layered perovskite increased by a factor of 10 as a result of exfoliation and restacking, 10 times the amount of Pt may also be needed to attain optimum activity.

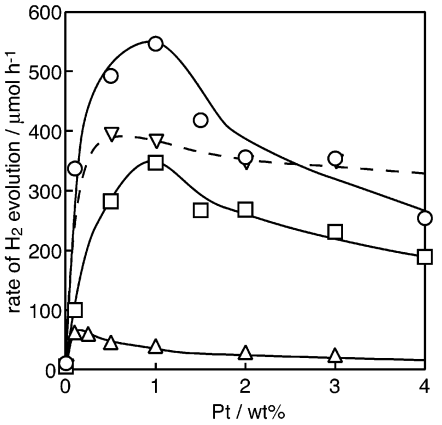

Figure 4. Photocatalytic activities of hydrogen gas generation as a function of Pt loading. (△) $KCa_2Nb_3O_{10}$; (○) *ex*-$Ca_2Nb_3O_{10}/K^+$; (□) *ex*-$Ca_2Nb_3O_{10}/Na^+$; (▽) TiO_2 (P-25).

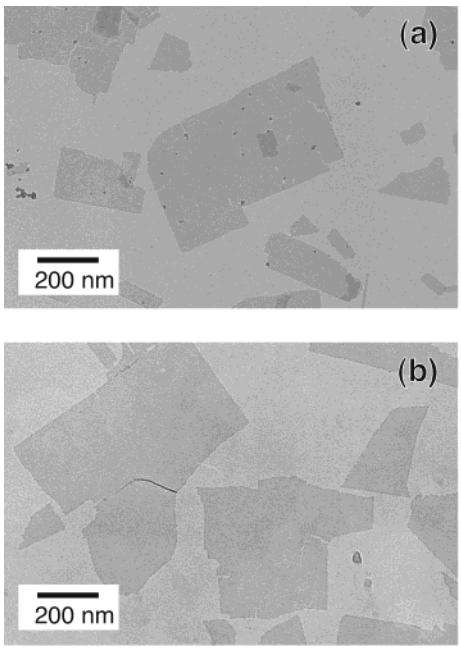

Figure 5. TEM images of $Ca_2Nb_3O_{10}$ nanosheets with Pt loading of (a) 3 wt % and (b) 0.1 wt %.

Photodeposition of Pt onto Nanosheets. It is highly important that Pt nanocrystallites can be deposited directly onto semiconductor nanosheets such as $Ca_2Nb_3O_{10}$ to obtain better control of the photochemical reaction activity. Figure 5 shows the TEM images of nanosheets after UV irradiation in H_2PtCl_6 solution. Very thin crystallites with uniform and faint contrast were found. This feature is characteristic of nanosheets, confirming that the unilamellar nature was maintained

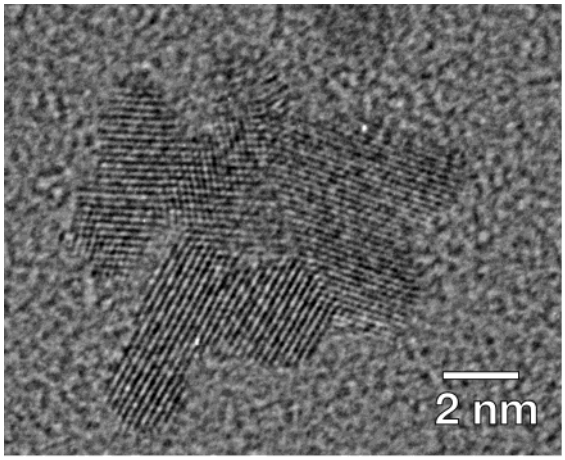

Figure 6. High-resolution TEM image of Pt particles deposited when 3 wt % of $PtCl_6^{2-}$ was applied.

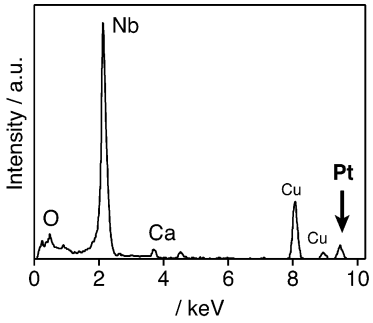

Figure 7. Local EDX spectrum for the nanosheet with Pt loading of 0.1 wt %. Electron beam diameter was ≈10 nm. Signals of Ca, Nb, and O are attributed to nanosheets. Peaks due to Cu are from the TEM grid.

even after photodeposition. Unlike a nanosheet sample without Pt deposition, there were several spots in high contrast on the nanosheets when 3 wt % of Pt was applied. The spots had an average size of ≈10 nm, and higher magnification revealed agglomerate particles (Figure 6). Each particle consisted of single crystals of several nanometers that showed clear lattice fringes. A lattice spacing of 0.2 nm was most frequently detected, which is in good agreement with the 200 lattice plane of Pt. Furthermore, EDX analysis detected Pt within the area surrounding the spots of high contrast. These results indicate that aggregated Pt nanocrystals can be deposited directly onto the perovskite nanosheets.

In contrast, when a smaller amount of Pt was photodeposited, TEM observation under low magnification did not detect Pt particles as spots in high contrast on the nanosheet (Figure 5b). However, an EDX scan with a probe diameter of about 10 nm detected a Pt signal in several areas. Figure 7 shows the local EDX spectrum of one of these areas. When these areas were observed under high-resolution TEM, fine particles of 1−2 nm were detected (Figure 8). The deposition of Pt was promoted via the reduction of $PtCl_6^{2-}$ by excited electrons generated in the $Ca_2Nb_3O_{10}$ nanosheets upon UV irradiation. When the concentration of $PtCl_6^{2-}$ is low, the reagent reacts with the photoexcited electrons immediately, yielding nanocrystals on the nanosheets. On the other hand, when a large amount of Pt is applied, excess $PtCl_6^{2-}$ not consumed in the initial stage may deposit onto Pt nanocrystals formed previously. Reduction of $PtCl_6^{2-}$ via this "crystal growth" may

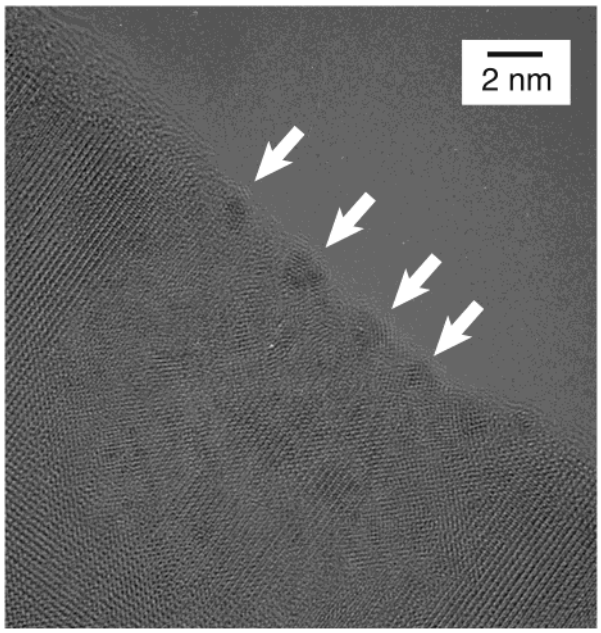

Figure 8. High-resolution TEM image of a Pt-loaded nanosheet (0.1 wt %). Arrows indicate possible locations of Pt nanoparticles that show slightly higher contrasts.

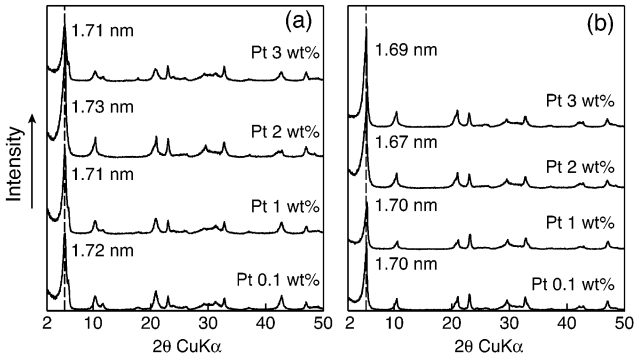

Figure 9. XRD patterns of restacked products of Pt-loaded nanosheets flocculated with (a) K^+ and (b) Na^+.

become predominant since photoexcited electrons easily migrate from the nanosheets to the Pt crystals and reduce the unreacted $PtCl_6^{2-}$. This process may bring about a difference in the morphology of the Pt deposited on the nanosheets.

Reassembling of Pt-Loaded Nanosheets. The Pt-loaded nanosheets were flocculated with KOH or NaOH solutions. Since Pt particles were randomly distributed on the nanosheet surfaces, most of the particles were expected to be accommodated within a nanosheet gallery. The flocculated products showed a lamellar structure with an intersheet spacing of 1.7 nm, similar to that of samples without Pt loading. The gallery height was not dependent on Pt loading (Figure 9). TEM observations definitely indicate that the Pt particles on the nanosheets grew beyond the intersheet distance. However, it is noteworthy that only a limited number of Pt nanocrystals were deposited on the nanosheet, leaving the remaining areas Pt-nanoparticle-free. In Pt-free areas, the strong electrostatic interaction between the interlayer ions (K^+ or Na^+) and nanosheets may hold the nanosheets tightly together, resulting in the intersheet distance of 1.7 nm. This indicates that Pt nanoparticles do not behave as "pillars", most likely due to

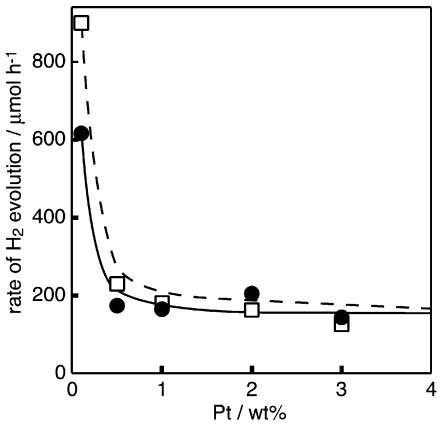

Figure 10. Hydrogen gas generation rate for restacked aggregates of Pt-loaded nanosheets. (●) *ex*-$Ca_2Nb_3O_{10}/K^+$; (□) *ex*-$Ca_2Nb_3O_{10}/Na^+$.

their scarcity. AFM and TEM images have also shown various nanosheets to be fairly flexible.[10,13,22]

Photocatalytic Activities for Restacked Aggregates of Pt-Loaded Nanosheets. Figure 10 shows photocatalytic activities of restacked samples of Pt-loaded nanosheets. High H_2 evolution rates, 620 and 900 μmol h^{-1}, were obtained for *ex*-$Ca_2Nb_3O_{10}/K^+$ and *ex*-$Ca_2Nb_3O_{10}/Na^+$ at a Pt loading of 0.1 wt %. These activities were higher than the activities of samples that were Pt-deposited after restacking. In addition, there is a noticeable difference in the dependence of Pt loading for the two systems. The activity drops significantly from 0.1 wt % Pt loading to 0.5 wt % and then plateaus with further Pt loading. This phenomenon contrasts with that of the samples Pt-loaded after restacking that showed increasing photocatalytic activity with increasing Pt loading. Photoexcited electrons migrate to Pt particles to reduce H^+ into H_2. In the samples loaded with Pt after restacking, Pt particles are expected to be located only on the surfaces of the restacked aggregates. The reduction efficiency of H^+ is expected to be lower since there are no Pt sites for electrons excited inside the aggregate. These excited electrons may be lost by recombining with positive holes. In contrast, the restacked aggregates of Pt-loaded nanosheets are expected to contain Pt nanoparticles that are highly dispersed throughout the sample, meaning Pt particles are expected to be present in the restacked nanosheet gallery as well as on the surface. This allows excited electrons to migrate easily to Pt particles nearby. However, an efficient evolution of H_2 gas was not observed experimentally except for very high efficiency for the sample with low Pt loading. The activity of ≈200 μmol h^{-1} that was observed was nearly half that observed for the other system. This phenomenon suggests that H_2 evolution via H_2O decomposition does not proceed within the intersheet space of the aggregates. A possible explanation for this is the limited or slow access of H_2O into the intersheet gallery from the aqueous solution outside. If this assumption is the case, the number of active sites on the surface may be smaller than that in the other system, which provides a reasonable explanation for the lower photocatalytic activities. A possible reverse reaction may also explain the results. The generated H_2 (or H atom) and oxidized species from methanol, for example, formaldehyde, are more or less confined in restricted nanosheet galleries, taking a longer time to escape from a reaction spot. They may be combined again on Pt, which may reduce the apparent rate of H_2 evolution.

The very high activities observed for the Pt loading of 0.1 wt % are peculiar. At 0.1 wt %, extremely small Pt single nanoparticles are deposited as described above. This state may be effective in H_2 generation from an aqueous methanol solution. A conclusion on this point must await further study.

Acknowledgment. The author would like to thank Mr. Keiji Kurashima for performing the TEM measurements and Mr. Satoshi Takenouchi for carrying out the chemical analysis. This work was supported by a grant for Core Research for Evolution Science and Technology (CREST).

Supporting Information Available: A chart of differential thermal analysis and thermogravimetry of the restacked perovskite nanosheets, *ex*-$Ca_2Nb_3O_{10}/K^+$ (PDF). This material is available free of charge via the Internet at http://pubs.acs.org.

CM020622E

(22) (a) Nadeau, P. H.; Wilson, M. J.; McHardy, W. J.; Tait, J. M. *Science* **1984**, *225*, 923. (b) Saupe, G. B.; Waraksa, C. C.; Kim, H.-N.; Han, Y. J.; Kaschak, D. M.; Skinner, D. M.; Mallouk, T. E. *Chem. Mater.* **2000**, *12*, 1556.